Titanium aluminide composites produced by laser melting

J. H. Abboud and D. R. F. West

The microstructures of titanium aluminide based composites have been investigated using optical microscopy, scanning electron microscopy, energy dispersive spectrometry, transmission electron microscopy, and scanning transmission electron microscopy. The composites were in the form of pellets of ~3 mm dia. produced by laser melting various mixtures of titanium, aluminium, and silicon carbide using 800 W laser power, 3 mm beam diameter, and 0·5 s pulse time. In all the processed samples, titanium and aluminium were completely melted and formed an alloy, whereas, SiC particles were partially dissolved leading to the enrichment of the alloy matrix with silicon and carbon. The aluminium contents of the matrixes of the composites spanned the range from ~15 to ~78 at.-%. In the 15–42 at.-%Al range, the phases formed during solidification were β titanium solid solution, TiC, and $Ti_5(Si,Al)_3$; β and $Ti_5(Si,Al)_3$ occurred together as a eutectic constituent. During solid state cooling, β phase transformed to either martensite or an $\alpha_2 + \gamma$ mixture, depending on the aluminium content of the matrix. At 57 at.-%Al the matrix solidified to form γ, TiC, and $Ti_5(Si,Al)_3$. The composite with 78 at.-%Al contained dendrites of $Ti(Al,Si)_3$ and interdendritic aluminium solid solution. Features of the Ti–Al–Si–C phase diagram are discussed in relation to the microstructures.

MST/1841

© *1994 The Institute of Materials.* *Manuscript received 29 January 1993; in final form 18 March 1993.* *The authors are in the Department of Materials, Imperial College of Science, Technology and Medicine, London.*

Introduction

Composites based on titanium based matrixes are currently attracting extensive interest in view of potential applications where enhanced properties such as specific strength and stiffness are required. A recent review by Flower and Clyne[1] has surveyed developments in the field; this includes processing aspects which are of particular importance in view of the significant reactions between titanium and reinforcement ceramic phases which occur during high temperature processing and which can cause degradation of properties.

One approach to the production of titanium based composites involves localised melting of material using high power continuous or pulsed lasers, and a number of investigations have been reported (e.g. Refs. 2–5). The injection of ceramic particles such as SiC or TiB_2 into laser generated melt pools has been used to produce surface composite layers ~0·5–1 mm in thickness with the aim of improving wear and erosion resistance. Another technique developed by Weerasinghe[6] produces composites in the form of small pellets, typically 1–3 mm dia., by pulsed laser melting mixtures of titanium and ceramic powder placed in a recess in a copper block; these pellets can potentially be consolidated via hot isostatic pressing to produce a bulk composite. In both methods the ceramic particles are partially dissolved leading to enrichment of the titanium with the products of the dissolution of the ceramic particles. For example, the injection of SiC particles into the laser melted zone of a β titanium alloy (Ti–15V–3Al–3Cr–3Sn) or laser melting of alloy powder with SiC leads to the formation of TiC dendrites at the SiC/matrix interface and in the matrix, and to the enrichment of the matrix with silicon and carbon.[4] The injection of TiB_2 into the laser melted zone of Ti–15V–3Al–3Cr–3Sn alloy or laser melting of alloy powder containing 20 vol.-%TiB_2 leads to the formation of TiB at the ceramic/matrix interfaces and in the matrix.[5] Some observations have also been reported on titanium aluminide composites containing 20 vol.-%SiC produced by melting powder mixtures containing titanium, aluminium, and silicon carbide.[5] The pellet technique provides a useful route to the investigation of the constitution of a range of multicomponent systems.

The present investigation has aimed to produce a series of titanium aluminide composite pellets spanning the composition range of Ti_3Al, TiAl, and $TiAl_3$ with particular emphasis on the microstructures and phase relationships.

Experimental procedure

Commercial purity (CP) titanium, aluminium (99·5%), and silicon carbide powders, of average particle sizes ~75, 75, and 150 μm respectively, were mixed together in a rotating mill for 1 h. A small amount of the mixture (~1 g) was placed in a recess of ~3 mm dia. in a copper block and melted using a pulsed CO_2 laser operated at 800 W, 3 mm beam diameter, and typically 0·5 s pulse time. The process was carried out in an atmosphere of argon gas to minimise contamination of the melted region. The product of laser melting is a small pellet of diameter dependent on laser power, pulse time, and the amount of the powder mixture. With the combination of laser conditions and the mass of powder used, the pellets were approximately spherical in shape. The cooling rates were relatively rapid and estimated to be of the order of 500 K s^{-1}. Figure 1 shows a typical example of a pellet[5] produced from a mixture of Ti–30 at.-%Al/20 vol.-%SiC, laser melted at 800 W power, 3 mm beam diameter, and 0·5 s pulse time. The average

Table 1 Average aluminium contents (at.-%) and hardness values of matrixes of Ti–Al composite pellets produced using pulsed laser operating conditions of 800 W, 3 mm beam diameter, and 0·5 pulse time

Pellet	Ti	Al	Si	C*	Hardness ± 20, HV0·5
1	71·5	15·0	6·7	~6·8	525
2	63·0	30·0	3·5	~3·5	530
3	55·5	32·0	6·0	~6·5	600
4	54·0	42·0	2·0	~2·0	620
5	37·5	57·5	2·5	~2·5	400
6	19·0	77·5	1·8	~1·7	270

* Carbon content was obtained by subtracting total proportion of other elements from 100%.

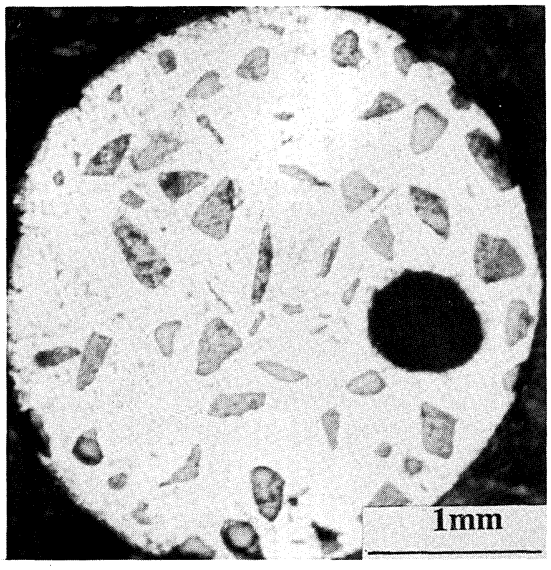

1 Typical pellet produced from mixture of titanium, aluminium, and SiC, laser melted at 800 W power and 0·5 s pulse time, showing partially dissolved SiC particles in aluminide matrix (From Ref. 5)

pellet diameter was ~3 mm and the distribution of the partially dissolved SiC particles was reasonably uniform.

Six mixtures were prepared containing a constant amount of SiC (15 wt-%) and aluminium contents of 10, 20, 23, 30, 47, and 65 wt-% respectively, spanning the range of titanium aluminides. Several pellets were produced from each mixture, mounted in bakelite, and prepared for metallography by grinding (from 120 to 1200 grit), polishing with alumina (from 5–0·05 μm), and etching with a solution of 2%HF, 10%HNO_3, and 88% distilled water. Scanning electron microscopy (SEM) linked with an energy dispersive spectrometer (EDS) was used for structural and compositional analysis. Thin foils were prepared for transmission (TEM) and scanning transmission electron microscopy (STEM), by grinding the pellet from both sides until a disc of ~200 μm thickness was obtained. The disc was dimpled from both sides until a thickness of ~50 μm was obtained. Ion beam thinning was used to obtain thin areas. X-ray diffractometry was carried out using Cu $K\alpha$ radiation. Microhardness measurements were made using a 500 g load on the matrix of the composites.

Results

MATRIX COMPOSITIONS

The average matrix compositions of the composite pellets produced with the various aluminium content mixtures are given in Table 1. All of the pellets show only partial solution of the SiC with consequent enrichment of the matrix in silicon and carbon. The results of EDS X-ray analysis of several areas (10 × 10 μm) on duplicate pellets were in good agreement. Analysis of the oxygen content of pellets of a Ti–Al alloy (without ceramic) yields values of 2300–2400 ppm.

MATRIX MICROSTRUCTURES

Pellet 1 (Ti–15Al–6·7Si–6·8C)

The microstructure (*see* Fig. 2*a*) shows a rim of reaction products around the SiC particles (~3 μm in extent) which was identified via EDS analysis as TiC and transformed β. The matrix consists predominantly of a two phase eutectic type structure with some titanium solid solution cells/

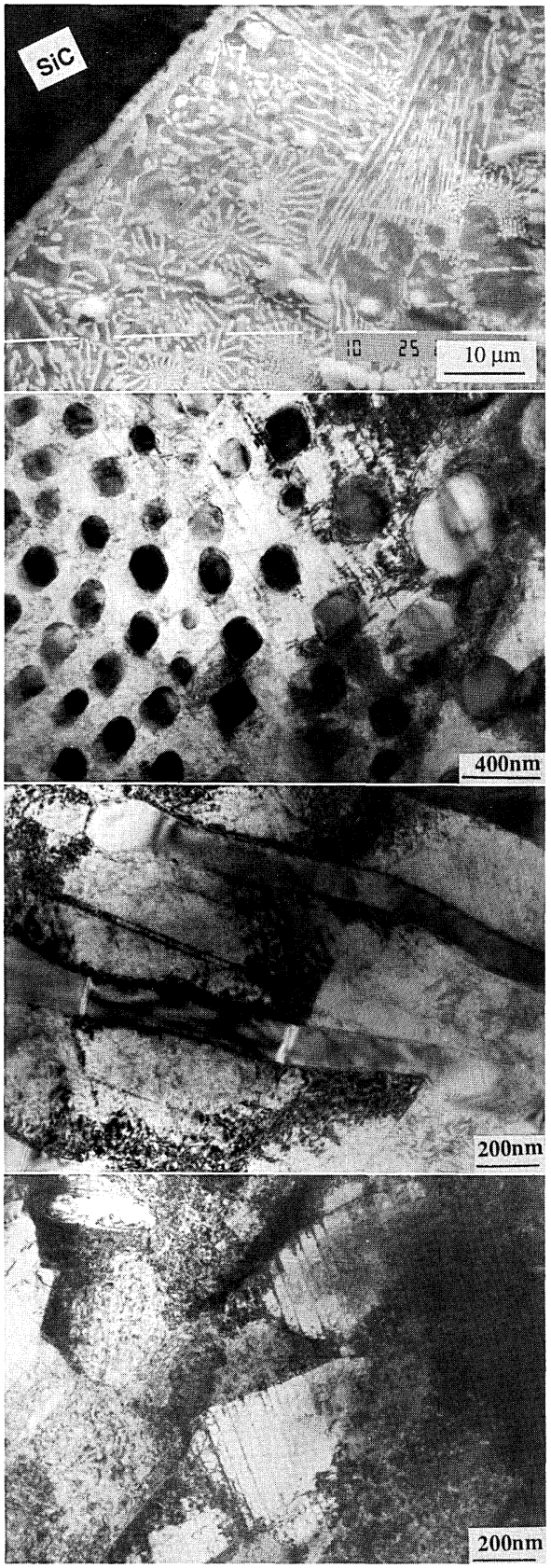

a partially dissolved SiC particles with reaction rim – matrix contains titanium solid solution cells/dendrites (α_2 martensite formed from β), eutectic α_2 martensite + $Ti_5(Si,Al)_3$, and TiC (SEM); *b*, *c* eutectic region (TEM); *d* martensite in prior β regions (TEM)

2 Pellet 1 (Ti–15Al–6·7Si–6·8C)

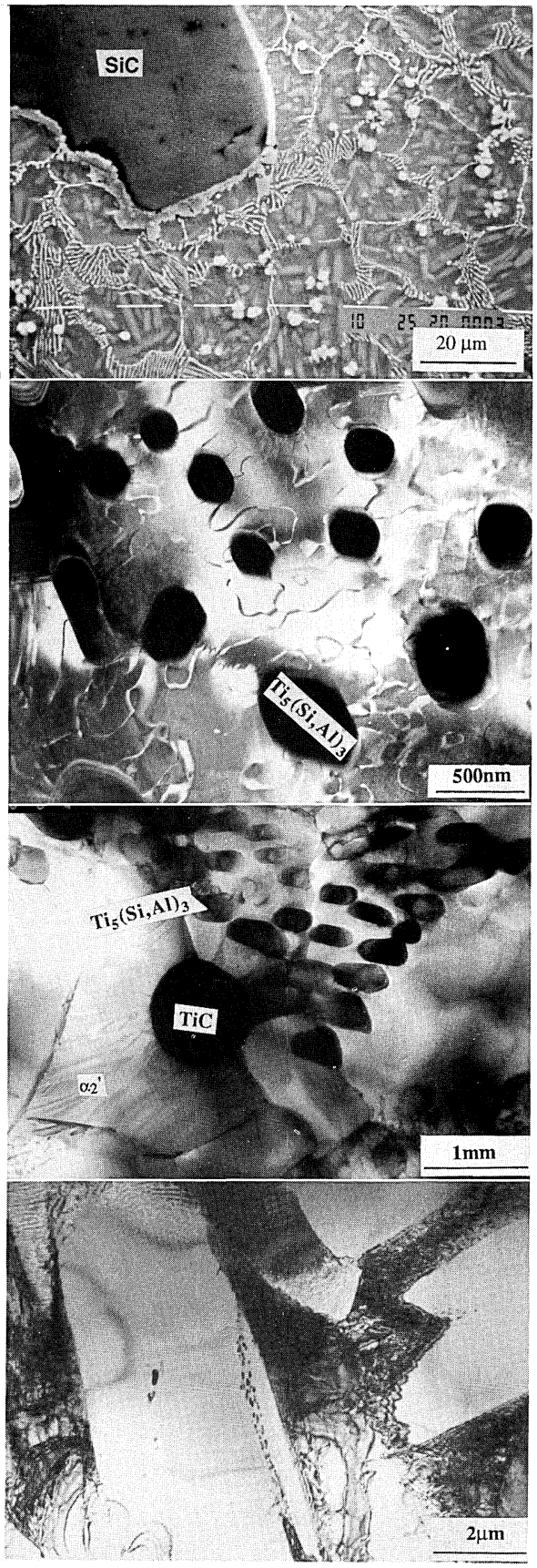

a partially dissolved SiC particle with reaction rim – matrix contains mainly cells/dendrites consisting of α_2 martensite (SEM); *b* eutectic α_2 martensite + $Ti_5(Si,Al)_3$ (TEM); *c* eutectic region and TiC particle (TEM); *d* martensite α_2' (TEM)

3 Pellet 2 (Ti–30Al–3·5Si–3·5C)

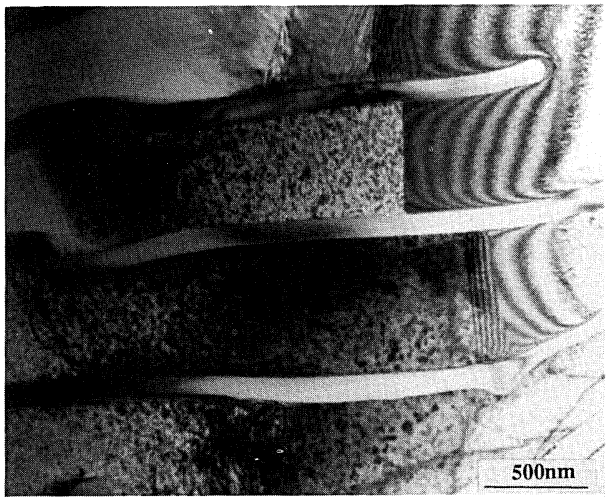

4 Pellet 3 (Ti–32Al–6·5Si–6·5C): eutectic region α_2 martensite + $Ti_5(Si,Al)_3$ is shown (TEM)

dendrites (*see* Fig. 2*a*). The spherical/dendritic particles were identified as TiC. Examination via TEM showed that the two phase eutectic regions consist of silicide particles with a hexagonal structure containing up to ~11%Al which were identified as $Ti_5(Si,Al)_3$, in a martensitic background (*see* Figs. 2*b* and 2*c*). Silicide particles show lamellar and rodlike morphologies in cross section. The silicide particle size ranges between 100 and 500 nm and the spacing between 200 and 500 nm. The titanium cells/dendrites consist of grains containing fine lath martensite (*see* Fig. 2*d*). The widths of the martensite laths range between 100 and 200 nm and they are typically aligned parallel to each other. Selected area diffraction patterns were indexed as hcp crystal structure with faint superlattice reflections. Attempts to reveal antiphase boundaries were unsuccessful.

Pellet 2 (Ti–30Al–3·5Si–3·5C)

The microstructure shows a substantial proportion of titanium solid solution cells/dendrites and some two phase eutectic structure; small TiC dendrites were found in the titanium solid solution dendrite areas and in the eutectic (*see* Fig. 3*a*). The rim around the SiC was identified via EDS analysis as transformed β and TiC, and was up to ~5 μm in extent. X-ray diffraction analysis showed the presence of Ti_3Al, TiC, and Ti_5Si_3. Examination via TEM showed that the eutectic regions consist of $\alpha_2' + Ti_5(Si,Al)_3$ (*see* Figs. 3*b*–3*d*). Selected area diffraction analysis confirmed the fcc structure and the hexagonal structure of the TiC and $Ti_5(Si,Al)_3$, respectively. Using STEM analysis it was shown that the latter compound contains ~11%Al. The martensite was of a lath type containing antiphase boundaries and a high density of dislocations (*see* Fig. 3*d*); some laths contained fine silicide particles. Selected area diffraction patterns from the martensite were indexed as hcp crystal structure with superlattice reflections.

Pellet 3 (Ti–32Al–6Si–6·5C)

The microstructure as observed using SEM is predominantly eutectic $\alpha_2' + Ti_5(Si,Al)_3$, similar to that observed in pellet 1. The rim around the SiC was ~3 μm in thickness and EDS analysis showed it to consist of TiC and transformed β. Studies, via TEM, of the eutectic show a range of morphologies, including lamellar structures, with frequent branching of the silicide lamellae and broken lamellae (*see* Fig. 4). Interlamellar spacings ranging from 100 to 500 nm are observed in different areas of the pellet. The regions between the silicides show fine subgrains

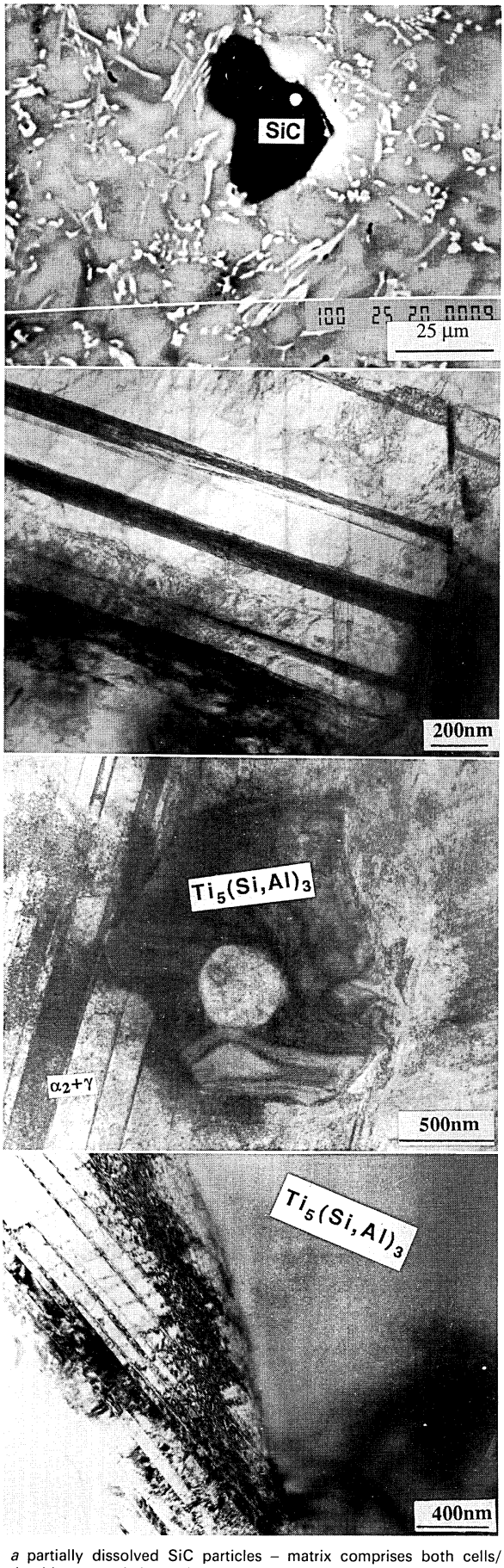

a partially dissolved SiC particles – matrix comprises both cells/dendrites consisting of $\alpha_2+\gamma$(Ti,Al) and faceted structure of $Ti_5(Si,Al)_3$ (SEM); *b* $\alpha_2+\gamma$ structure within cells/dendrites (TEM); *c*, *d* $\alpha_2+\gamma+Ti_5(Si,Al)_3$ intercells/dendrites (TEM)

5 Pellet 4 (Ti–42Al–2Si–2C)

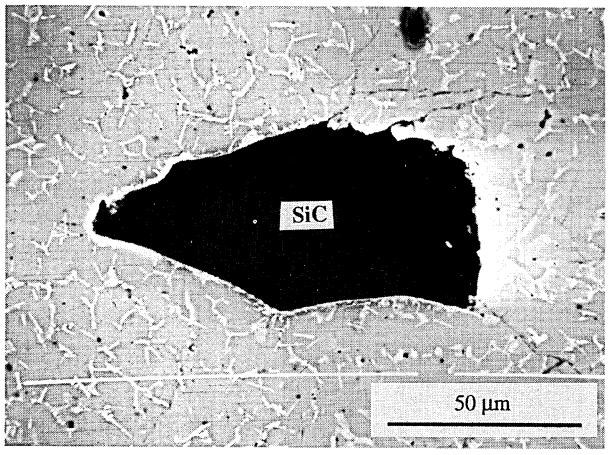

6 Pellet 5 (Ti–57·5Al–2·5Si–2·5C): partially dissolved SiC particle with reaction rim is shown – matrix comprises cells/dendrites of γ and eutectic $\gamma+Ti_5(Si,Al)_3$ (back scattered SEM)

containing antiphase boundaries. The $Ti_5(Si,Al)_3$ has a similar composition to that in pellets 1 and 2.

Pellet 4 (Ti–42Al–2Si–2C)

The microstructure shows cells/dendrites of titanium solid solution with intercellular/dendritic regions containing some lamellar eutectic and some relatively large faceted silicide particles (*see* Fig. 5*a*). No rim around the SiC was observed. By examining the microstructure using TEM and selected area diffraction, it was shown that cells/dendrites consist of fine lamellae of α_2 and γ whose interphase spacings were about 50 nm (*see* Fig. 5*b*); the intercellular/dendritic regions show $\alpha_2+\gamma+Ti_5(Si,Al)_3$ (*see* Fig. 5*c*). The silicide particles are coarse and have the same composition and crystal structure as those in pellets 1–3 (*see* Fig. 5*d*).

Pellet 5 (Ti–57·5Al–2·5Si–2·5C)

The microstructures show a cellular/dendritic structure of TiAl phase (γ) and intercellular/dendritic eutectic regions consisting of $\gamma+Ti_5(Si,Al)_3$ which show some lamellar morphology (*see* Fig. 6); small TiC particles were also observed with the eutectic regions. The constitution of the rim around SiC particles was not determined. Results were not obtained using TEM because the preparation of thin foils was very difficult due to cracks in the specimen.

Pellet 6 (Ti–77·5Al–1·8Si–1·7C)

The microstructure consists of dendrites containing ~74%Al and intercellular/dendritic regions rich in aluminium (*see* Fig. 7*a*). The rim around the SiC particles was about 2–4 μm in extent and consisted of TiC. Examination via EDS, TEM, and STEM showed the dendrites to be $Ti(Al,Si)_3$, containing a high density of dislocations (*see* Fig. 7*b*) whereas the interdendritic regions were aluminium based solid solution.

Phase diagram of Ti–Al–Si–C system

The phase diagram for the quarternary Ti–Al–Si–C system does not appear to have been reported in the literature. However, on the basis of data for the constituent binary and ternary systems, certain features can be represented semischematically relevant to the solidification and solid state constitution of the materials rich in titanium and aluminium studied in the present work. Figure 8 shows a

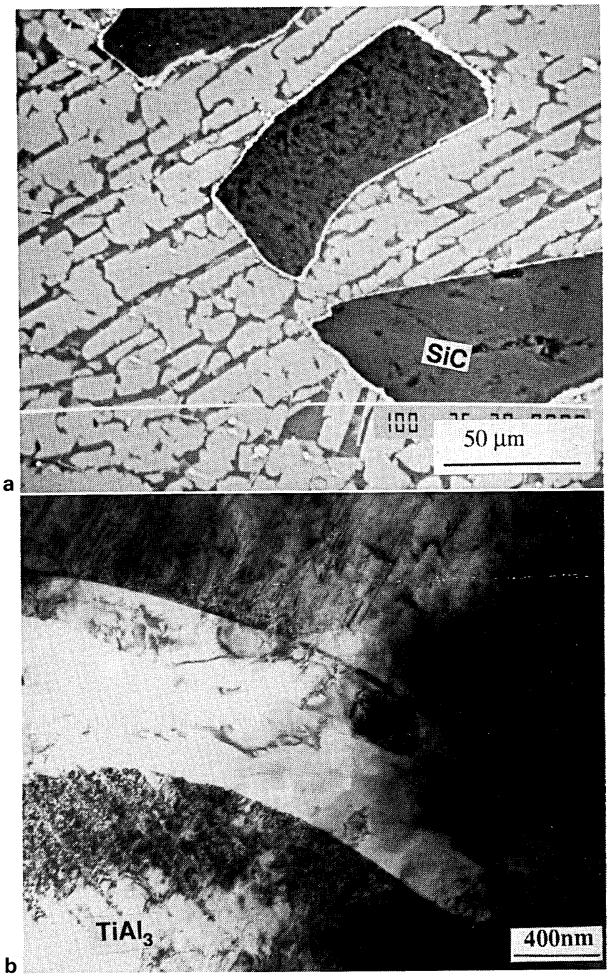

a partially dissolved SiC particles with reaction rim – matrix contains $TiAl_3$ dendrites and aluminium solid solution (SEM); *b* $TiAl_3$ dendrite with high density of dislocations (TEM)

7 Pellet 6 (Ti–77·5Al–1·8Si–1·7C)

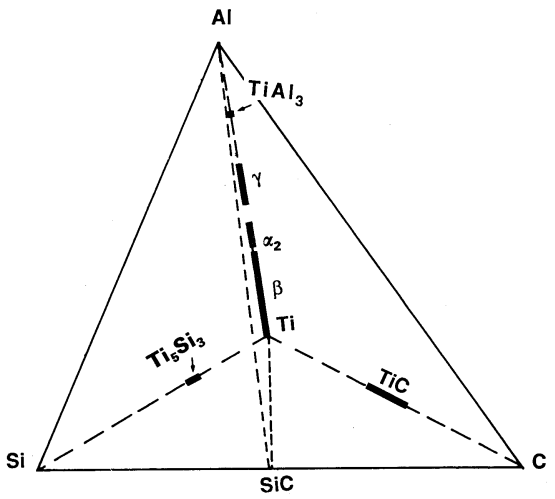

8 Semischematic diagram of Ti–Al–Si–C system showing phases at ~1200°C relevant to present work

tetrahedron representing an isothermal section at a high temperature (~1200°C) with the compounds that have been encountered in the present work, namely, TiAl(γ), $TiAl_3$, TiC, and $Ti_5(Si,Al)_3$. The primary solid solutions, α and β, based on titanium, and the aluminium based solid solution are also shown. However, the compound Ti_3Al (α_2) which is encountered in the composites, being formed martensitically during solid state cooling at lower temperatures, is not indicated.

Figure 9 amplifies Fig. 8 by means of partial isothermal sections for the constituent ternary systems Ti–Al–C, Ti–Si–C, Ti–Al–Si, and Al–Si–C. The Ti–Al–Si partial section is based on data for 1200°C determined by Khataee *et al.*[7] Wu *et al.*[8] reported a solubility of 2–3%Si in Ti_3Al. The Ti–Al–C data shown in Fig. 8 were reported by Cam *et al.*[9] as a partial isothermal section at 1250°C. The Ti–Si–C phase fields shown in Fig. 8 are based on the isothermal section at 1200°C reported by Brukl.[10] Features of the Al–Si–C system[11] include a three phase Al–Si–SiC region, a binary carbide (Al_4C_3) and two ternary carbides designated as P and H (P is shown in Fig. 9).

To assist in interpreting the evolution of the matrix microstructure during solidification, Fig. 10 shows a semischematic representation of part of the liquidus projection of the Ti–Al–Si–C system. The perspective looks towards the titanium rich corner of the composition tetrahedron, and liquidus features are shown for the ternary systems Ti–Al–C, Ti–Al–Si, and Ti–Si–C. Table 2 summarises the compositions of various microstructural constituents.

The Ti–Al–C liquidus is based on that presented by Cam *et al.*,[9] which was deduced from previous work reported in the literature[12,13] and from microscopical observations on as solidified alloys. The Ti–C system contains the stable carbide TiC, existing over a wide range of compositions ~37–49%; the phase diagram[14] shows another form of carbide, Ti_2C, in which vacancies are ordered on the carbon sublattice. The eutectic at ~1650°C is shown as $L \rightarrow \beta + Ti_2C$.[14] In the present paper, the carbide is designated TiC and the eutectic as $L \rightarrow \beta + TiC$. The representation of the Ti–Al–Si liquidus projection incorporates the experimental observations of Wu *et al.*[8] who determined part of a liquidus valley associated with the eutectic reaction; $L \rightarrow \beta$ (transformed to α'_2 in the solid state) + $Ti_5(Si,Al)_3$; the composition range of this valley was from ~18–33%Al and ~5–9%Si, and eutectic temperatures around 1500°C were found, decreasing slightly with decreasing Al content. The reaction curve shown in Fig. 10 is drawn on the assumption that this eutectic valley runs down to the $L \rightarrow \beta + Ti_5Si_3$ reaction in the binary Ti–Si system.

The part of the Ti–Si–C liquidus shown in Fig. 10 has been deduced from binary system data and from microstructural observations previously reported[4,5] on laser produced composites containing SiC and based on commercial purity titanium alloy (Ti–6Al–4V) and a β alloy (Ti–15V–3Cr–3Sn–3Al); these composites were produced as pellets and/or surface layers. The proposed form of the

Table 2 Compositions (SEM–EDS) of cell/dendrites and eutectic containing silicide, at.-%

Pellet	Position	Ti	Al	Si	C
1	β dendrites, PA	75·5	21·5	1·5	1·5
	$\beta + Ti_5(Si,Al)_3$ eutectic, AA	77·0	15·0	7·5	0·5
	Dendrites + eutectic + TiC	71·5	15·0	6·7	6·8
2	β dendrites, PA	66·8	32·5	1·0	0·7
	$\beta + Ti_5(Si,Al)_3$ eutectic, AA	64·0	28·5	7·0	0·5
	Dendrites + eutectic + TiC	63·0	30·0	3·5	3·5
3	β dendrites, PA	64·0	35·0	0·7	0·3
	$\beta + Ti_5(Si,Al)_3$ eutectic, AA	60·5	33·0	6·5	...
	Dendrites + eutectic + TiC	55·5	32·0	6·0	6·5
4	β dendrites, PA	54·5	44·5	1·0	...
	$\beta + Ti_5(Si,Al)_3$ eutectic, AA	56·0	40·0	4·0	...
	Dendrites + eutectic + TiC	54·0	42·0	2·0	2·0
5	γ dendrites, PA	39·0	60·0	0·5	0·5
	$\gamma + Ti_5(Si,Al)_3$ eutectic, AA	40·0	53·7	6·3	...
	Dendrites + eutectic, AA	37·5	57·5	2·5	2·5
6	$TiAl_3$ dendrites, PA	26·5	72·0	1·5	...
	Dendrites + interdendritic, AA	19·0	77·5	1·8	1·7

PA point analysis; AA area analysis.

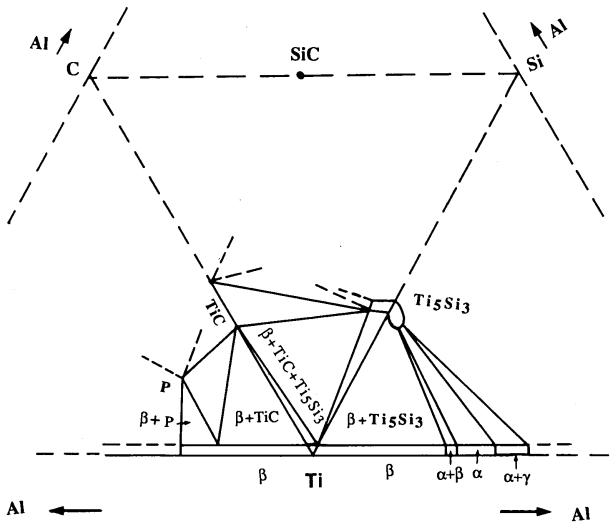

9 Partial isothermal section data for constituent ternary systems of Ti–Al–Si–C system based on Ti–Al–C (1250°C, Ref. 9); Ti–Si–C (1200°C, Ref. 10); Ti–Al–Si (1200°C, Ref. 7); and Al–Si–C (Ref. 11)

liquidus, as shown in Fig. 10 has three univariant reaction curves; one derives from the $L \rightarrow \beta + TiC$ eutectic in the binary Ti–C system, one from the $L \rightarrow \beta + Ti_5Si_3$ eutectic in the Ti–Si system, and the third is suggested to be $L \rightarrow TiC + Ti_5Si_3$. An invariant reaction is shown at the junction of the three univariant curves, and is suggested to be a eutectic; $L \rightarrow \beta + TiC + Ti_5Si_3$. In the Ti–SiC composites studied[3,4] the phases encountered were β titanium (transformed to martensite in the solid state, or, in the case of the β alloy, retained as metastable β phase), Ti_5Si_3, and TiC. Typically the average matrix microstructure contained about 5–7%Si, with the equivalent proportion of carbon, derived from partial solution of the SiC particles. Observations of the microstructure suggest that TiC formed as the primary phase, which is in accord with the proposed liquidus. As TiC forms, the liquid composition changes until it encounters the L, β titanium, TiC univariant curve. The microstructure shows that β formed as cells/dendrites, which may correspond to a divorced eutectic morphology. Alternatively, it was suggested that the univariant curve, in this composition range, may be peritectic in nature; $L + TiC \rightarrow \beta$; if this is so, with incomplete reaction due to the rapid solidification, β phase will form as the liquid composition changes over the β liquidus. The presence of a lamellar structure of transformed $\beta + Ti_5Si_3$ was interpreted as resulting from the liquid composition encountering the $L \rightarrow \beta + Ti_5Si_3$ eutectic valley. The microstructural observations showed some rounded particles of TiC, associated with this lamellar eutectic. It was suggested that this TiC forms as part of the ternary eutectic, constituting only a small proportion of the eutectic, assuming that the ternary eutectic composition is very close to the Ti–Si axis, as depicted in Fig. 10; the TiC particles might therefore be a divorced product of the eutectic. However, it has not been proved conclusively that this TiC was not the primary phase. In the composites based on the β titanium alloy it was found that with silicon contents of ~2% in the matrix, the eutectic containing silicide did not form, since the silicon remained in solution in the retained β phase.[14]

Discussion

SOLIDIFICATION SEQUENCES OF PELLETS 1–6

In the present work compositional data required for correlation with the microstructure can be represented in terms of the Ti–Al–SiC section (*see* Fig. 11) through the quaternary tetrahedron shown in Fig. 8. The average compositions of the composite pellets are shown as points (*) on the lines joining the SiC corner of the triangle to positions on the Ti–Al side, corresponding to the proportions of titanium and aluminium; this assumes that no preferential loss of any of the elements occurred during laser processing. Additionally, Fig. 11 shows the average compositions of the solute enriched matrixes of the various pellets (as given in Table 1) determined by EDS analysis of

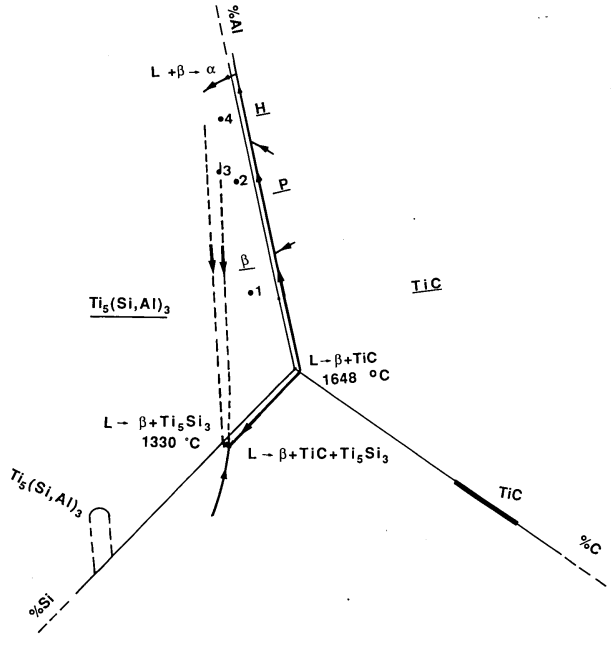

10 Semischematic diagram of liquidus projection of part of Ti–Al–Si–C system showing phases relevant to present work and approximate composition of matrixes of pellets 1–4: H and P are ternary carbides in Ti–Al–C system[7] (primary phase regions are underlined, e.g. H)

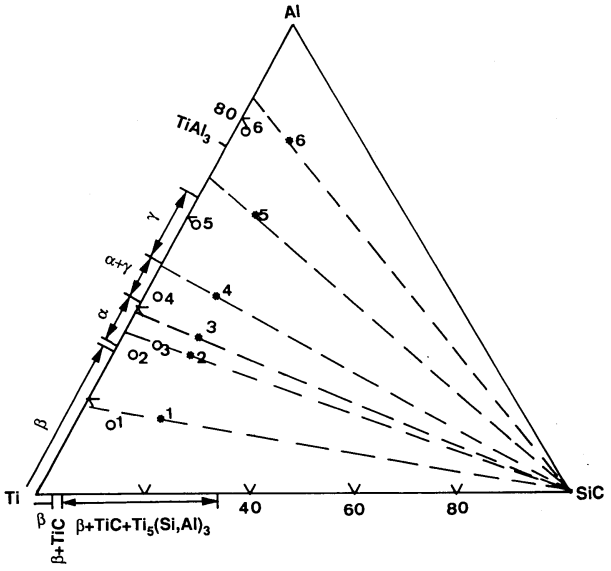

11 Ti–Al–SiC section of Ti–Al–Si–C system showing average compositions (*) of composite mixtures and of matrixes (○) of pellets 1–6 (*see* Table 1): positions of some boundaries of phase region in Ti–Al and Ti–SiC section at ~1200°C are also shown

representative areas incorporating all the phases present; (although SiC is not present as a constituent in the matrix, the silicon and carbon contents are plotted as mol.-%SiC). These compositions also should lie on the same lines as the average compositions of the pellets, neglecting the presence of the reaction zones around the SiC particles whose compositions are not known. The aluminium contents of the matrixes are lower than the line would suggest, indicating loss of aluminium during processing. The proportions of silicon and carbon in the matrix of a given pellet should be equal, and the data in Table 1 are in reasonable agreement with this, indicating that no consistent trend to preferential loss of either of these elements occurs during laser processing.

Application of the lever rule to the average compositions of the pellets and the matrixes on the Ti–Al–SiC lines in Fig. 11 shows the extent of solution of SiC particles during processing. Although the power density and the pulse time were the same for each pellet, the extent of solution of SiC was not the same in each pellet, being greatest for pellets 1 and 3; pellets 2 and 4 show less solution and pellets 5 and 6 even smaller effects. The origin of these differences is not properly understood.

Figure 11 also shows some of the solid state phase boundaries at ~1200°C for the Ti–Al system and for the Ti–SiC section of the Ti–Si–C system (derived from Fig. 9). The number of phases involved and the occurrence of solid state transformations on cooling produce a complex arrangement of phase fields in the quaternary system, and the compositions of the individual phases do not lie in the plane of the section. However, the information in Fig. 11 assists in depicting the constitution of the composite pellets.

In pellets 1–4, whose matrix compositions lie in the range ~15–42%Al, with ~7–2%Si and C (Table 1) the solidification sequence gives rise to the same three phases, namely β titanium solid solution, TiC, and $Ti_5(Si,Al)_3$, in addition to undissolved SiC particles. The aluminium in the matrix exists mainly in solid solution in the β phase, which also contains small proportions of silicon in solution (maximum ~3·5% in titanium and ~1·5% in α_2'). The β phase transformed during solid state cooling either to ordered martensite or, at the highest matrix aluminium content (42%) to a mixture of $\alpha_2 + \gamma$ (as discussed below). TiC also contains small proportions of aluminium and silicon in solution. The pellets showing the greatest extent of SiC solution (i.e. 1 and 3) have the highest silicon and carbon contents in the matrix and will be expected to show higher proportions of $Ti_5(Si,Al)_3$ and TiC than the other pellets. The silicide content in the form of the eutectic is clearly greater in pellets 1 and 3, consistent with this (*see* Figs. 2*a* and 3*a*); pellet 4 has a lower silicon content than pellets 1–3 and a low silicide content. The proportion of TiC is less than ~10 vol.-% in all three pellets, and pellet 2 appears to have slightly less carbide than do 1 and 3; no TiC was detected in pellet 4.

Concerning the solidification sequences of pellets 1 and 3 which have similar structures, it is difficult to deduce with certainty whether β titanium or TiC is the primary phase. For example, in Fig. 1 some of the TiC particles appear to be surrounded by β, suggesting that the carbide forms first; on the other hand some carbide particles appear to be closely associated with the silicide eutectic. The predominance of the eutectic, however, indicates that the matrix composition lies very close to the liquidus surface representing the equilibrium of liquid, β and $Ti_5(Si,Al)_3$ (*see* Fig. 10). In pellet 2 where the lower silicon and carbon contents lead to the predominance of β phase, it is uncertain whether β is the primary phase or whether the small proportion of TiC formed first.

The overall solidification sequences are suggested to broadly follow that discussed above for the Ti–SiC composites,[4] bearing in mind, however, that the β phase in the present study contains high proportions of aluminium. In pellets 1–3, if TiC forms first, the liquid composition would reach the liquid, β, TiC liquidus surface, possibly representing a peritectic reaction $L + TiC \rightarrow \beta$; this reaction will not proceed significantly, but the liquid composition will move through the $L + \beta$ region to encounter the L,β, silicide surface; possibly some TiC may form in association with the β + silicide eutectic in the ternary eutectic reaction which completes the solidification. In pellet 2 the lower silicon content leads to the formation of β cells/dendrites as the main feature of the solidification sequence. In pellet 4, the low silicon content also leads to a predominance of primary β and the solidification is completed by the β + silicide eutectic; the fact that TiC was not detected indicates that all, or virtually all, of the carbon is in solution. For the higher aluminium content of pellet 5, γ is the primary phase; γ replaces β in the subsequent stages of solidification involving the eutectic containing silicide.

The solidification sequence of pellet 6 differs fundamentally from those of pellets 1–4, since the very high aluminium content of the matrix (~78%) leads to $Ti(Al,Si)_3$ being the dominant phase. The phase relationships are complex, involving several intermetallic compounds and solid state transformations, including the formation of long period superlattices. Schuster and Ipsen[15] have recently reported a detailed reinvestigation of this part of the system and showed greater complexity than that in the phase diagram as assessed by Murray.[14] Their work confirms that $TiAl_3$ forms peritectically by the reaction of liquid with Ti_5Al_{11} (designated in the diagram assessed by Murray), but two other peritectic reactions leading to the formation of $TiAl_2$ and $Ti_{1-x}Al_{1-x}$ are reported at temperatures above that of the $L + \delta \rightarrow TiAl_3$ reaction. In pellet 6, with a matrix containing ~78%Al, equilibrium solidification should commence with the formation of $TiAl_2$ and then Ti_5Al_{11} before the formation of $TiAl_3$. However, with the rapid solidification of the pellets, the extent of the peritectic reactions preceding the formation of $TiAl_3$ will be restricted and $TiAl_3$ formation will dominate until solidification is completed by the formation of aluminium solid solution. The microscopical studies carried out in the present work did not detect compounds other than $TiAl_3$, but the presence of a small proportion of $TiAl_2$ and/or Ti_5Al_{11} is a possibility; also the presence of silicon may modify the phase relationships so that these compounds do not form.

$\beta + Ti_5(Si,Al)_3$ EUTECTIC

The composition data for the liquidus valley of the β + silicide eutectic obtained in the present work (*see* Table 2) agree well with those previously reported by Wu *et al.*[8] and Es-Souni *et al.*[16] for the ternary Ti–Al–Si system; the maximum solubility of aluminium in the silicide found in the present work, namely ~11%, is lower than that previously reported, namely up to 13%. The previous studies[16,17] of the silicide eutectic in ternary Ti–Al–Si alloys, including some in the rapidly solidified condition have shown a range of morphologies, with colonies of silicide lamellae or rods. Studies using TEM[16,17] showed interphase spacings in the range 70–200 nm, and features such as 'broken' lamellae and overlapping and branching lamellae. The silicide lamellae were found to nucleate on β cells and to grow to form complex structures. The occurrence of a range of spacings was interpreted as characteristic of 'irregular' eutectics incorporating a faceted phase (i.e. the silicide) whose growth is anisotropic and is affected by planar surface defects. It was suggested[17] that the eutectic coupled zone is skewed towards the faceted phase so that high undercooling can lead to the appearance of cellular β dendrites with second phase 'segregates'.

The present observations show features similar to those in the previous work, including the occurrence of a range of spacings and branching of lamellae. Figure 2*a* shows the development of eutectic colonies, with evidence that, in some cases, they originate from β regions. Areas of rod shaped silicide are commonly present at the centres of approximately spherical shaped colonies, whereas the outer regions are suggestive of a lamellar morphology. In Fig. 3*a*, where the proportion of the eutectic in the pellet is relatively small, the eutectic forms in the intercellular/dendritic regions of the primary β. In pellet 4 which also contains a relatively small amount of intercellular/dendritic eutectic the morphology includes larger silicide plates with a smaller proportion of regions showing coupled growth (*see* Fig. 5); this may originate from the fact that the matrix composition of pellet 4 has the highest aluminium and lowest silicon contents of pellets 1–4. The β phase, which is predominant in the eutectic, is characterised by the presence of dislocations, which may be attributed to stresses generated during solid state cooling from mismatch of thermal expansion coefficient. In pellet 5 where γ phase is the basis of the eutectic, the $Ti_5(Si,Al)_3$ morphology in some regions resembles the lamellar structure found in the β + silicide eutectic of pellets 1–3.

SOLID STATE TRANSFORMATIONS

The main solid state transformation to be considered is that in the β titanium solid solution; the aluminium content of the β, which ranges up to ~42% in the pellet matrixes, will be influential in determining the nature and morphology of the transformation product for the cooling rates encountered. Previously reported work[18] on laser surface alloyed Ti–Al layers has shown that ~15%Al martensite forms with a predominantly lath type morphology and with some evidence of ordering detected by selected area diffraction. With increasing aluminium content, α'_2 ordered martensite forms showing antiphase boundaries. There is a transition in morphology, with substantial amounts of acicular martensite and some massive transformation product occurring with increase in aluminium content. The M_s temperature increases with aluminium content, and a possible mechanism for the transition was suggested. In the present work, pellets 1–4 showed that ordered martensite, formed during cooling of β. The superlattice selected area diffraction pattern reflections from the matrix (15%Al) in pellet 1 were too weak to image the antiphase boundaries, but these were seen in pellets 2–3 (e.g. *see* Fig. 3*b*). In pellet 1 the original β areas, when observed using TEM (*see* Fig. 2*c*), showed subgrains (~5 μm in size) within which martensite laths formed in parallel as bundles. For pellet 2 (30%Al), which contained a large volume fraction of β, the SEM (*see* Fig. 3*a*) shows larger martensite laths, not in bundles. Es-Souni *et al.*[16] have previously reported the existence of retained β phase (ordered) within the eutectic regions in a Ti–29Al–6·5Si alloy. It was suggested that nucleation of martensite is favoured by the lamellar structure, due to stress accumulation at the β/silicide interface; however, martensite growth can be impeded by the resistance to shear offered by a matrix containing large undeformable particles with small spacings so that M_s could be lowered. No evidence of retained β was obtained in the present work. In pellet 4, whose matrix contained 42%Al, solid state cooling led to the formation of fine lamellar structures (*see* Fig. 5) consisting of α_2 and γ as expected from phase diagram considerations. In pellet 6, the high dislocation density (*see* Fig. 7) may indicate the occurrence of solid state transformation.

HARDNESS

The data in Table 1 for pellets 1–4 with matrixes containing 15–42%Al and with silicon and carbon contents in the range ~2–7% show high hardness values (525–620 HV); the structures of pellets 1–3 consisted of martensite + $Ti_5(Si,Al)_3$ + TiC whereas pellet 4 contained no TiC but some γ (as part of $\alpha'_2 + \gamma$ lamellar structure). Data for laser surface alloyed binary Ti–Al alloys showed high values of 410, 475, 500, 525, and 300 for 17, 23, 30, 43, and 50%Al, respectively[18] but these values are lower than those of the Ti–Al–Si–C alloy matrixes.

In the binary Ti–Al system,[18] the high hardness of the martensite is attributed to a combination of solid solution effects: ordering (antiphase boundaries), size of the martensite laths or plates, and high dislocation density and is also due to oxygen in solution; at 42% the $\alpha'_2 + \gamma$ lamellae are expected to contribute significantly to hardness.

In the Ti–Al–Si–C system, martensite is the major structural constituent in pellets 1–3, formed both within the β cells and in the eutectic regions. The hardness of the martensite increased with aluminium content, and silicon and carbon in solution may contribute additionally by solid solution strengthening. Further strengthening resulting from the fine duplex eutectic mixture of martensite + $Ti_5(Si,Al)_3$ is also expected; TiC (having hardness of the order of 2000 HV), although present only in small proportions, will contribute further to the hardness. In pellets 1 and 3, which contain similar proportions of phases, the high hardness of pellet 3 may be attributed to the higher aluminium content. In pellet 2, although the martensite is harder than in pellet 1, there is a smaller proportion of eutectic. In pellet 4, the high aluminium content of α_2 and the fine $\alpha_2 + \gamma$ lamellae contributed substantially to the hardening. The hardness (400 HV) of pellet 5 was associated with γ phase (which is softer than Ti_3Al), $Ti_5(Si,Al)_3$, and TiC. The hardness (270 HV) of pellet 6 is associated with a predominantly $TiAl_3$ structure.

Conclusions

Composites containing SiC particles in a matrix of titanium aluminides can be produced as approximately spherical pellets, up to ~3 mm dia. by laser melting powder mixtures of Ti, Al, and SiC. With selected laser processing conditions complete melting of the titanium and aluminium occurs, but with only partial solution of the SiC; the matrix of the composite is enriched in silicon and carbon. With matrixes containing ~15–42 at.-%Al, the phases formed during solidification were β titanium solid solution, TiC, and $Ti_5(Si,Al)_3$. The relatively rapid solidification of the pellets yields refined microstructures. The primary solidification involves either β phase or TiC phase followed by a univariant reaction involving liquid, β, and TiC, and then a eutectic $L \rightarrow \beta + Ti_5(Si,Al)_3$. The structure of this eutectic showed a range of morphologies including colonies of fine lamellae or rods of silicide. Particles of TiC were observed in association with the eutectic containing silicide and solidification may be completed by an invariant eutectic: liquid $\rightarrow \beta + Ti_5(Si,Al)_3 + TiC$. In the composite whose matrix contained 57·5 at.-%Al, the primary and dominant phase is γ. At an aluminium content of ~78 at.-%Al the structure consists mainly of $Ti(Al,Si)_3$. Ternary phase diagram data provide a basis for interpreting the matrix structures in the context of the Ti–Al–Si–C system.

During solid state cooling, β phase transforms to ordered α_2 martensite or at 42 at.-%Al, to an $\alpha_2 + \gamma$ lamellar structure. At 78 at.-%Al, the substructural features suggest the occurrence of a solid state transformation.

For matrix aluminium contents of 15–42 at.-%Al, the hardness values of 525–620 HV obtained were attributed mainly to solid solution strengthening of the martensite and strengthening from a fine scale structure associated with the eutectic containing silicide and $\alpha_2 + \gamma$ lamellae.

Acknowledgements

The authors would like to acknowledge the SERC for financial support and IMI Titanium Ltd for carrying out the oxygen analysis.

References

1. H. FLOWER and T. W. CLYNE: in Proc. 'Seventh world conference on titanium', San Diego, CA, July 1992, TMS.
2. J. D. AYERS: 'Lasers in metallurgy', (ed. K. Mukherjee and J. Mazumder), 279; 1981, Warrendale, PA, The Metallurgical Society of AIME.
3. J. H. ABBOUD and D. R. F. WEST: *J. Mater. Sci. Lett.*, 1991, **10**, 1149–1152.
4. J. H. ABBOUD and D. R. F. WEST: *Mater. Sci. Technol.*, July 1989, **5**, 725–728.
5. J. H. ABBOUD and D. R. F. WEST: in Proc. 'Seventh world conference on titanium', San Diego, CA, July 1992, TMS.
6. V. WEERASINGHE: unpublished work, Imperial College of Science, Technology and Medicine, 1989.
7. A. KHATAEE, H. FLOWER, and D. R. F. WEST: unpublished work, Imperial College of Science, Technology and Medicine, 1989.
8. J. S. WU, P. A. BEAVAN, and R. WAGNER: *Scr. Metall.*, 1990, **24**, 207–212.
9. G. CAM, H. FLOWER, and D. R. F. WEST: *Mater. Sci. Technol.*, June 1991, **7**, 505–511.
10. C. E. BRUKL: 'Ternary phase equilibria in transition metal–boron–carbon–silicon systems', Part 2, Vol. 7, Technical report AFML/TR/65/2, US Department of Commerce, Springfield, VA (*see* also P. Martineaeu, R. Pailler, M. Lahaye, and R. Naslain: *J. Mater. Sci.*, 1984, **19**, 2749–2720).
11. L. L. ODEN and R. H. McCUNE: *Metall. Trans.*, 1987, **18A**, 2005–2014.
12. J. C. SCHUSTER, H. NOWOTNY, and C. VACARO: *J. Solid State Chem.*, 1980, **32**, 213–219.
13. A. M. ZAKHAROV, L. A. LASHKOVA, and S. E. SEMERYAKOVA: *Russ. Metall.*, 1987, **4**, 196–1197.
14. J. MURRAY: 'Binary alloy phase diagrams', (ed. T. B. Massalski), 173–176; 1986, Metals Park, OH, ASM.
15. J. SCHUSTER and H. IPSEN: *Z. Metallkd.*, 1990, **80**, (6), 389–396.
16. M. ES-SOUNI, P. A. BEAVAN, and R. WAGNER: *Scr. Metall. Mater.*, 1990, **24**, 2175–2180.
17. M. ES-SOUNI, R. WAGNER, and P. A. BEAVAN: *Mater. Sci. Eng.*, 1992, **A151**, 69–75.
18. J. H. ABBOUD and D. R. F. WEST: *Mater. Sci. Technol.*, September 1991, **7**, 827–834.

New ... New ... New ... New ... New ... New ... New ... New ...

Optical Materials

Roger M Wood

This book has been written as an introduction to the theory and use of optical materials (excluding glasses) and should be of interest to anyone studying or working in the optics and electro-optics fields, including sixth form students, undergraduates, post-graduates, teachers and lecturers.

Starting with a review of the relationship between a material's atomic, molecular and crystallographic structure, electromagnetic theory and the resulting linear and non-linear optical properties, the author then goes on to apply this insight to such subjects as optical non-linear effects, lasers, detectors, integrated optics and fibres and liquid crystals. The text ends with a discussion of the power-handling properties of optical materials.

Contents

- ✷ Introduction
- ✷ Molecular and Crystal Structure
- ✷ Physical Properties
- ✷ Optical Properties of Linear Materials
- ✷ Optically Non-Linear Materials
- ✷ Laser Materials
- ✷ Detector Materials
- ✷ Fibre / Integrated Optics
- ✷ Liquid Crystals
- ✷ Power Handling Capability of Optical Materials

Book 553 246x172mm 122pp 0 901716 44 8 Hard 1993 £25.00 US$50.00

Orders with remittance* to: The Institute of Materials, Sales & Marketing Dept., 1 Carlton House Terrace, London SW1Y 5DB. Tel. (071) 976 1338 Fax. (071) 839 2078.
Credit cards accepted.
***Carriage: EC customers add £3.50 per order; Non-EC customers add US$8.00**
Members of The Institute of Materials receive a 20% discount on this title.